JOURNAL OF COMPUTATIONAL PHYSICS 95, 359–386 (1991)

Chebyshev Collocation Solutions of the Navier–Stokes Equations Using Multi-domain Decomposition and Finite Element Preconditioning

P. DEMARET* AND M. O. DEVILLE

Université Catholique de Louvain,
Unité de Mécanique Appliquée, Louvain-La-Neuve, Belgium

Received April 4, 1989; revised February 8, 1990

The steady Navier–Stokes equations are solved using series of basis functions involving Chebyshev polynomials. The projection method is a collocation scheme. A Newton's linearization is performed in order to obtain a set of algebraic equations. As the matrix system is ill conditioned, the collocation technique is preconditioned by a standard Galerkin finite element method using a 9-nodes Lagrangian element which presents decisive advantages: sparsity, reduced condition number, easy treatment of complicated geometries. To handle nontrivial geometries in the collocation process, a domain decomposition is set up. The treatment of interface conditions is fully described. Several test problems like the regularized driven square cavity and the backward facing step are discussed to show the abilities of the present algorithm. © 1991 Academic Press, Inc.

1. INTRODUCTION

In this paper, the steady Navier–Stokes equations are solved in primitive variables formulation using basis functions involving Chebyshev polynomials. Spectral schemes have various choices of projection methods: Galerkin, Tau, collocation [2]. Here, we deal with the collocation technique because the computation is fully performed in the physical domain. Moreover, collocation is able to treat nonconstant coefficients as well as to set up easily the discrete equations.

Orthogonal collocation is a global process and produces full matrices. For second-order elliptic problems, Deville and Mund [11] showed the structure of such matrices. As they present a condition number $O(N^4)$ if N is the number of degrees of freedom for a one-dimensional problem, the collocation method is preconditioned. Two major families of preconditioners appeared in the literature over the last decade. Finite differencing (FD) first was proposed independently by Y. Morchoisne [19] and S. A. Orszag [20]. FD preconditioning was used primarily with the Richardson iterative method. It was shown by Haldenwang *et al.* [13] that for the Laplace equation, the spectrum of $L_{ap}^{-1} L_C$ is in between 1 and $\pi^2/4$, where

* Now with Solvay S.A., Brussels.

0021-9991/91 $3.00
Copyright © 1991 by Academic Press, Inc.
All rights of reproduction in any form reserved.

L_{ap} denotes the approximate FD operator and L_C the collocation approximation of the continuous L operator. Therefore, the Richardson method must be under-relaxed. In the mid-eighties, Canuto and Quarteroni [4] and Deville-Mund [10] performed finite element (FE) preconditioning for elliptic problems. Deville and Mund [11] demonstrated numerical evidence of the FE superiority as preconditioner compared to FD. It is now known that for linear elements, the presence of the mass matrix helps reducing the spectrum of $L_{ap}^{-1}L_C$ by a factor of 3. FE preconditioning converges (at least) twice as fast as FD preconditioning [2]. In the context of standard Galerkin FE methods, Demaret and Deville [7] showed that for the Stokes equations, the classical 9-nodes Lagrangian element is the best preconditioner for the global solution coupling the momentum and continuity equations.

Up to now, low-order preconditioning was used to speed up the iterative convergence of high-order methods. However, one can adopt another point of view which is the iterative defect correction method [11]. Here, the high-order residual evaluation accelerates the discretization error reduction and yields improved accuracy if the solution is smooth enough.

The 9-nodes Lagrangian preconditioner is applied in the present paper to the Navier–Stokes equations. A Newton's linearization is carried out on the continuous equations. Then, the collocation approximation is described and the resulting linearized discrete equations are introduced. The collocation equations are preconditioned by the FE method. As the weak formulation automatically incorporates natural boundary conditions, a domain decomposition may be designed. The physical domain is divided into several macro-domains. Here, the interfaces must be parallel to the coordinate axis. Interface conditions are based on jumps of the stress vectors and are included in the variational problem. At convergence, the collocation method achieves C^1 continuity of the global solution for smooth problems. This is probably the most striking difference between the present method and the spectral element technique [18].

The extension of the collocation method to thermal problems is done in [8]. The method was applied to the simulation of thermal convection arising in the industrial process of a molten glass furnace [9].

Section 2 gives the basic equations. In Section 3, the mathematical tools are defined. Section 4 presents the collocation technique and the preconditioned iterative approach. The algorithm is described in Section 5. The domain decomposition is analyzed in Section 6. Section 7 reports numerical results for the mono-domain approach while Section 8 deals with multi-domain calculation and discusses the pros and cons of mono- versus multi-domain computations.

2. Basic Equations

In this paper, we will deal with the steady state Navier–Stokes equations written in stress formulation:

$$\rho(\mathbf{u}\cdot\nabla)\mathbf{u} = \operatorname{div}\boldsymbol{\sigma} + \rho\mathbf{f}, \tag{2.1.a}$$

$$\boldsymbol{\sigma} = -p\mathbf{I} + 2\mu\mathbf{d}, \tag{2.1.b}$$

$$\mathbf{d} = \tfrac{1}{2}[\nabla\mathbf{u} + (\nabla\mathbf{u})^{\mathrm{T}}], \tag{2.1.c}$$

$$\operatorname{div}\mathbf{u} = 0, \tag{2.1.d}$$

where $\mathbf{u}$ denotes the velocity field, p the pressure, μ the dynamic viscosity, $\mathbf{f}$ the body forces, $\boldsymbol{\sigma}$ the stress tensor, $\mathbf{I}$ the unit tensor, $\mathbf{d}$ the rate of deformation tensor. The superscript T indicates the transpose. Equation (2.1.a) is the momentum equation while Eq. (2.1.d) enforces the continuity constraint for incompressible fluids. All boldface quantities are vectors; those that are boldface sans serif are tensors.

Equations (2.1) are solved on the domain Ω. The boundary conditions are given by the relationship

$$B\mathbf{u} = \mathbf{g} \qquad \text{on} \quad \partial\Omega, \tag{2.2}$$

where $\partial\Omega$ represents the boundary of the domain Ω. The boundary conditions are of two kinds. Essential (Dirichlet) boundary conditions are applied on $\partial\Omega_e$:

$$\mathbf{u}(\mathbf{r}) = \mathbf{g}_1(\mathbf{r}), \qquad \forall\mathbf{r}\in\partial\Omega_e. \tag{2.3}$$

In (2.3), $\mathbf{r}$ denotes the position vector. On $\partial\Omega\backslash\partial\Omega_e = \partial\Omega_n$, natural boundary conditions apply:

$$\mathbf{t}(\mathbf{r}) = \boldsymbol{\sigma}\cdot\mathbf{n} = \mathbf{g}_2(\mathbf{r}), \qquad \forall\mathbf{r}\in\partial\Omega_n. \tag{2.4}$$

In (2.4), $\mathbf{t}$ is the stress vector which is related to the stress tensor $\boldsymbol{\sigma}$ through the Cauchy principle (first equality in (2.4)). Here, $\mathbf{n}$ is the unit outward normal vector to $\partial\Omega_n$.

As Eq. (2.1.a) is nonlinear, a Newton's linearization process is set up. Assuming the Fréchet derivatives of the Navier–Stokes operator exist and denoting by $\delta\mathbf{u}$ and $\delta\boldsymbol{\sigma}$ the variations of the velocity field and the stress tensor, respectively, the linearized Navier–Stokes equations are

$$\rho[(\mathbf{u}^n\cdot\nabla)\,\delta\mathbf{u} + (\delta\mathbf{u}\cdot\nabla)\,\mathbf{u}^n] - \operatorname{div}\delta\boldsymbol{\sigma} = \operatorname{div}\boldsymbol{\sigma}^n + \rho\mathbf{f}^n - \rho(\mathbf{u}^n\cdot\nabla)\,\mathbf{u}^n, \tag{2.5.a}$$

$$\operatorname{div}\delta\mathbf{u} = -\operatorname{div}\mathbf{u}^n, \tag{2.5.b}$$

$$\mathbf{u}^{n+1} = \mathbf{u}^n + \delta\mathbf{u}, \qquad \boldsymbol{\sigma}^{n+1} = \boldsymbol{\sigma}^n + \delta\boldsymbol{\sigma}, \tag{2.5.c}$$

where the superscript refers to the iteration index of the Newton's scheme. Equations (2.5) are solved with the following boundary conditions:

$$\delta\mathbf{u} = 0, \qquad \forall\mathbf{r}\in\partial\Omega_e, \tag{2.6}$$

and

$$\delta\mathbf{t} = \delta\boldsymbol{\sigma}\cdot\mathbf{n} = -\mathbf{t}^n + \mathbf{g}_2(\mathbf{r}), \qquad \forall\mathbf{r}\in\partial\Omega_n. \tag{2.7}$$

3. Notations and Definitions

In this paper, we use the same notations as in [7]. Let us denote by N the couple $(N_{x_1}, N_{x_2}) \in \mathfrak{N} \times \mathfrak{N}$, where $\mathfrak{N}$ is the set of natural numbers. The discrete Chebyshev mesh $\mathfrak{G}_N$ results from the cartesian product of one-dimensional Gauss-Lobatto–Chebyshev (GLC) quadrature grids,

$$\mathfrak{G}_N = \bigotimes G_{x_i, N_{x_i}}, \qquad i = 1, 2, \tag{3.1}$$

with $G_{x_i, N_{x_i}}$ being the roots of the equation:

$$(1 - x^2)\, T'_{N_{x_i}} = 0, \qquad x \in [-1, 1]. \tag{3.2}$$

In (3.2), $T'_{N_{x_i}}$ is the derivative of the Chebyshev polynomial of first kind and degree N_{x_i}. As a consequence, the GLC grid is built upon the abscissae:

$$x_k = \cos \frac{\pi k}{N_{x_i}}, \qquad k \in [0, N_{x_i}]. \tag{3.3}$$

Following Ciarlet [5], $\mathfrak{R}_N$ is the collection of rectangles whose vertices coincide with four neighbouring gridpoints of $\mathfrak{G}_N$ such that $\mathfrak{R}_N = \bigcup_i R_i$. Let $\mathfrak{P}_{(n,n)}$ denote the space of 2-rectangles of type (n) or two-dimensional Lagrangian finite elements which are restricted to nth degree interpolants over each rectangle $R_i \in \mathfrak{R}_N$. Here, we will restrict ourselves to $n = 1, 2$. The space $\mathscr{P}_N$ will contain all the continuous functions in $\bar{\Omega} = \Omega \cup \partial\Omega$, which are polynomials of degree N_{x_i} in the x_i variable.

Because of the finite element preconditioning of the Chebyshev collocation scheme, we need to define a few FE spaces. The velocities will come from

$$V_{2,h} = \{ v_h \in C^0(\bar{\Omega}) \,|\, \forall R_i \in \mathfrak{R}_N,\ v_{h|R_i} \in \mathfrak{P}_{(2,2)} \}, \tag{3.4}$$

while the pressure belongs to

$$P_{1,h} = \{ q_h \in L^2(\bar{\Omega}) \,|\, \forall R_i \in \mathfrak{R}_N,\ q_{h|R_i} \in \mathfrak{P}_{(1,1)} \}. \tag{3.5}$$

Given a smooth continuous functions $\mathbf{g}_1$ on $\partial\Omega_e$, $V_{2,h}(\mathbf{g}_1)$ will be the affine space of the functions in $V_{2,h}$ which correspond to $\mathbf{g}_1$ at the essential boundary nodes:

$$V_{2,h}(\mathbf{g}_1) = \{ v_h \in V_{2,h} \,|\, v_h(\mathbf{r}_b) = \mathbf{g}_1(\mathbf{r}_b),\ \forall \mathbf{r}_b \in \mathfrak{G}_{2,N} \cap \partial\Omega_e \}. \tag{3.6}$$

If the function $\mathbf{g}_1$ vanishes, the corresponding subspace will be denoted by $V^0_{2,h}$.

In (3.6), the grid $\mathfrak{G}_{n,N}$ is the set of global nodes for the FE mesh in Ω generated by the 2-rectangles of type (n), $n = 1, 2$. For $n = 1$, $\mathfrak{G}_{1,N} \equiv G_N$. The case $n = 2$ consists in the classical 9-nodes Lagrangian element [7]. Associated with these meshes, a set of linear functionals $1_{\mathfrak{G}_{n,N}}$ is defined on the global grid $\mathfrak{G}_{n,N}$. At the element level, this set corresponds to an nth degree bivariate Lagrange interpolation problem.

Now, we need to introduce some interpolation operators for the FE technique. The notation I_h will denote the FE interpolation on the Lagrangian basis functions:

$$I_h = \begin{cases} I_{2,h}^v : C^0(\bar{\Omega}) \to V_{2,h} & \\ (I_{2,h}^v \mathbf{v})(\mathbf{r}_i) = 1_{\mathfrak{G}_{2,N}} \mathbf{v}(\mathbf{r}_i), & \forall \mathbf{r}_i \in \mathfrak{G}_{2,N} \\ I_{1,h}^q : C^0(\bar{\Omega}) \to P_{1,h} & \\ (I_{1,h}^q q)(\mathbf{r}_i) = 1_{\mathfrak{G}_{1,N}} q(\mathbf{r}_i), & \forall \mathbf{r}_i \in \mathfrak{G}_N. \end{cases} \tag{3.7}$$

In (3.7), $I_{2,h}^v$ and $I_{1,h}^q$ are the velocity and the pressure interpolators, respectively. A particular case occurs when velocities satisfy essential boundary conditions. Using the notation I_h^e, we have

$$I_h^e = \begin{cases} I_{2,h}^v : C^0(\bar{\Omega}) \to V_{2,h} & \\ (I_{2,h}^v \mathbf{v})(\mathbf{r}_i) = 1_{\mathfrak{G}_{2,N}} \mathbf{v}(\mathbf{r}_i), & \forall \mathbf{r}_i \in \mathfrak{G}_{2,N} \cap (\bar{\Omega} \backslash \partial\Omega_e) \\ \quad = \mathbf{g}_1(\mathbf{r}_i), & \forall \mathbf{r}_i \in \mathfrak{G}_{2,N} \cap \partial\Omega_e \\ I_{1,h}^q : C^0(\bar{\Omega}) \to P_{1,h} & \\ (I_{1,h}^q q)(\mathbf{r}_i) = 1_{\mathfrak{G}_{1,N}} q(\mathbf{r}_i), & \forall \mathbf{r}_i \in \mathfrak{G}_N. \end{cases} \tag{3.8}$$

On $\partial\Omega_n$, stresses are computed by the interpolation operator $\mathfrak{I}_h$ defined as follows:

$$\mathfrak{I}_h = \begin{cases} [-1_{\mathfrak{G}_{1,N}} p(\mathbf{r}_i) + 2\mu 1_{\mathfrak{G}_{2,N}} \mathbf{d}(\mathbf{r}_i)] \cdot \mathbf{n} = \mathbf{g}_2(\mathbf{r}_i), & \forall \mathbf{r}_i \in \mathfrak{G}_{2,N} \cap \partial\Omega_n \\ 0, & \forall \mathbf{r}_i \in \mathfrak{G}_{2,N} \cap \partial\Omega_c. \end{cases} \tag{3.9}$$

For the sake of brevity, we shall use a scalar product notation for elements in $L^2(\Omega)$:

$$(u, v) = \int_\Omega u(\mathbf{r})\, v(\mathbf{r})\, d\Omega.$$

On the spectral side, spectral interpolation operators will act from a set of nodal values into $\mathscr{P}_N$. The spectral interpolator I_N is defined by the relations:

$$I_N = \begin{cases} I_N^v : C^0(\bar{\Omega}) \to \mathscr{P}_N & \\ (I_N^v \mathbf{v})(\mathbf{r}_i) = \mathbf{v}(\mathbf{r}_i), & \forall \mathbf{r}_i \in \mathfrak{G}_N \\ I_N^q : C^0(\bar{\Omega}) \to \mathscr{P}_N & \\ (I_N^q q)(\mathbf{r}_i) = q(\mathbf{r}_i), & \forall \mathbf{r}_i \in \mathfrak{G}_N. \end{cases} \tag{3.10}$$

4. Collocation Method and Finite Element Preconditioning

4.1. *Chebyshev Collocation*

We use orthogonal collocation in the framework of the weighted residual methods [2]. The residuals to the p.d.e.'s and to the boundary conditions are obtained inserting finite developments of the dependent variables (velocity, pressure) in terms of basis functions $h_i(x_i)$. Denoting by u_N such a dependent variable, one has

$$u_N = \sum_{i=0}^{N_{x_1}} \sum_{j=0}^{N_{x_2}} u_{ij} h_i(x_1)\, h_j(x_2) \tag{4.1}$$

with

$$\begin{aligned} h_i(z) &= \frac{(1-z^2)\, T'_{N_z}(z)(-1)^{i+1}}{\bar{c}_i N_z^2 (z - z_i)}, \qquad && i \in [0, N_z], \\ \bar{c}_0 = \bar{c}_{N_z} &= 2; \ \bar{c}_i = 1, && \forall i \in [1, N_z - 1]. \end{aligned} \tag{4.2}$$

The basis functions satisfy the orthogonality property,

$$h_i(z_k) = \delta_{ik}, \tag{4.3}$$

where δ_{ik} is the Kronecker symbol.

It should be noted that the interpolant used in (4.1) is the same as the one used by Patera [21] in the Chebyshev spectral element. This equivalence is based on the identity

$$\sum_{n=0}^{N} \frac{T_n(x_j)\, T_n(x)}{\bar{c}_n} = \frac{(1-x^2)\, T'_N(x)(-1)^{j+1}}{2N(x - x_j)}.$$

The projection method imposes that the scalar product of the residuals with Dirac functions vanishes. Denoting by Res_N these residuals, one obtains

$$(\mathrm{Res}_N(\mathbf{r}_i), \delta(\mathbf{r} - \mathbf{r}_i)) = 0, \qquad \forall \mathbf{r}_i \in \mathfrak{G}_N. \tag{4.4}$$

Here, the collocation nodes are those of the GLC grid. Applying the collocation procedure to the linearized equations (2.5)–(2.7), the discrete equations are obtained:

$$\begin{aligned} &\{ -\nabla\, \delta p + 2 \operatorname{div} \mu\, \delta \mathbf{d} - \rho[(\delta \mathbf{u} \cdot \nabla)\, \mathbf{u}^n + (\delta \mathbf{u}^n \cdot \nabla)\, \delta \mathbf{u}] \}(\mathbf{r}_i) \\ &\quad = \{ \nabla p^n + \rho(\mathbf{u}^n \cdot \nabla)\, \mathbf{u}^n - 2 \operatorname{div} \mu \mathbf{d}^n + \rho \mathbf{f}^n \}(\mathbf{r}_i) \\ &\operatorname{div} \delta \mathbf{u}(\mathbf{r}_i) = -\operatorname{div} \mathbf{u}^n(\mathbf{r}_i), \qquad \forall \mathbf{r}_i \in \mathfrak{G}_N \cap \Omega, \\ &\quad \delta \mathbf{u}(\mathbf{r}_i) = 0, \qquad \forall \mathbf{r}_i \in \partial\Omega_e \cap \mathfrak{G}_N, \\ &\quad \delta \mathbf{t}(\mathbf{r}_i) = \mathbf{g}_2(\mathbf{r}_i) - \mathbf{t}^n(\mathbf{r}_i), \qquad \forall \mathbf{r}_i \in \partial\Omega_n \cap \mathfrak{G}_N. \end{aligned} \tag{4.5}$$

Introducing L_C^{LNS} and L_C^{NS} the linearized Navier–Stokes operator in the left-hand side of (4.5) and the Navier–Stokes operator in the right-hand side, respectively, the matrix system corresponding to (4.5) takes the form,

$$L_C^n \, \delta \mathbf{x} = \mathbf{b}^n, \tag{4.6}$$

where

$$\begin{aligned} &\delta \mathbf{x} = (\delta \mathbf{u}, \delta p)^T, \\ &L_C^n = \begin{pmatrix} -L_C^{LNS}(\mathbf{x}) \\ B_C \end{pmatrix}, \qquad \mathbf{b}^n = \begin{pmatrix} L_C^{NS} \\ \mathbf{b}^{bc} \end{pmatrix} \mathbf{x}^n, \\ &\mathbf{b}^{bc} = \begin{pmatrix} \mathbf{0} \\ \mathbf{g}_2 - \mathbf{t}^n \end{pmatrix}, \\ &\mathbf{x} = (\mathbf{u}^n, p^n)^T. \end{aligned} \tag{4.7}$$

In (4.7), B_C is the collocation approximation of the boundary conditions expressed in (4.5). We notice that the right-hand side of (4.6) is the residual to the governing equations expressed at the old iteration level.

The solution of (4.6) presents some major drawbacks: as the Chebyshev collocation technique is a global method, the matrix involves a large bandwidth; furthermore, the viscous part of the operator is conditioned as $O(N^4)$ (if N is the number of degrees of freedom for a 1D problem) compared to $O(N^2)$ for standard finite differences or FE methods. Therefore, the collocation system is preconditioned by FE in order to decrease the condition number and to benefit from existing codes with lower computational work [11].

4.2. *Finite Element Preconditioning*

The numerical scheme is based on the preconditioned Richardson iteration technique:

$$\hat{L}(\delta \mathbf{x}^{k+1} - \delta \mathbf{x}^k) = -\alpha_k (L_C^n \, \delta \mathbf{x}^k - \mathbf{b}^n), \tag{4.8}$$

where

$$\hat{L} = L_{FE}$$

is a finite element approximate operator. In (4.8), the superscript k denotes the Richardson index. The initial guess of (4.8) is computed by

$$\delta \mathbf{x}^0 = I_N \mathbf{y}_h, \tag{4.9}$$

where $\mathbf{y}_h$ is the solution of the FE problem: Find $\mathbf{y}_h = (\delta \mathbf{u}_h, \delta p_h)^T$ in $V_{2,h}^0 \times P_{1,h}$ such that

$$
\begin{aligned}
&a_0(\delta \mathbf{d}_h, \mathbf{v}_h) + a_1(\delta \mathbf{u}_h; \mathbf{u}_h^n, \mathbf{v}_h) + a_1(\mathbf{u}_h^n; \delta \mathbf{u}_h, \mathbf{v}_h) - (\delta p_h, \operatorname{div} \mathbf{v}_h) \\
&\quad = -a_0(\mathbf{d}_h^n, \mathbf{v}_h) - a_1(\mathbf{u}_h^n; \mathbf{u}_h^n, \mathbf{v}_h) + (p_h, \operatorname{div} \mathbf{v}_h) \\
&\qquad + a_2(\mathbf{g}_2 - \mathbf{t}_h^n, \mathbf{v}_h) + (\rho \mathbf{f}_h^n, \mathbf{v}_h), \\
&-(q_h, \operatorname{div} \delta \mathbf{u}_h) \\
&\quad = (q_h, \operatorname{div} \mathbf{u}_h), \qquad \forall \mathbf{v}_h, q_h \in V_{2,h} \times P_{1,h}, \qquad \forall \mathbf{g}_2 \in L^2(\bar{\Omega}).
\end{aligned} \tag{4.10}
$$

The operators a_i, $i = 0, ..., 2$, are defined:

$$
\begin{aligned}
a_0(\mathbf{d}_h, \mathbf{v}_h) &= \mu(\nabla \mathbf{u}_h, \nabla \mathbf{v}_h) + \mu[(\nabla \mathbf{u})_h^{\mathrm{T}}, \nabla \mathbf{v}_h], \\
a_1(\mathbf{w}_h; \mathbf{u}_h, \mathbf{v}_h) &= \rho((\mathbf{w}_h \cdot \nabla)\, \mathbf{u}_h, \mathbf{v}_h), \\
a_2(\mathbf{u}_h, \mathbf{v}_h) &= \int_{\partial \Omega_n} \mathbf{u}_h \mathbf{v}_h \, dl.
\end{aligned}
$$

The subsequent iterations are carried out using the relationship:

$$
\delta \mathbf{x}^{k+1} = \delta \mathbf{x}^k - \alpha_k I_N (L_{\mathrm{FE}}^n)^{-1} [I_h^e (L_{\mathrm{C}}^n \, \delta \mathbf{x}^k - \mathbf{b}^n), \mathfrak{I}_h(\delta \mathbf{t}^k + \mathbf{t}^n - \mathbf{g}_2)]. \tag{4.11}
$$

The convergence of (4.8) or (4.11) depends strongly on the eigenvalue spectrum of $L_{\mathrm{FE}}^{-1} L_{\mathrm{C}}$. For the Stokes operator, Demaret and Deville [7] showed that the 9-nodes Lagrangian element yields an optimum rate of convergence when α_k is set to the value $\frac{2}{3}$. For the Navier–Stokes operator, the first-order derivatives are approximated by centered schemes when the standard Galerkin method is applied. In [12], Deville and Mund show that for the FE preconditioning of the first-order derivative by quadratics, static condensation on a uniform mesh leads to a staggered scheme. The Fourier analysis yields a spectrum for $L_{\mathrm{FE}}^{-1} L_{\mathrm{C}}$ which is bounded unlike the FD case and is in the range $[1, \pi/4]$. Using this result as a guideline for the Chebyshev case, the relaxation parameter is slightly decreased with increasing Reynolds number.

5. Algorithm

The preconditioned linearized Navier–Stokes equations (4.11) present two nested iterative procedures. The outer loop drives the Newton's scheme on the linearized equations, while the inner loop performs the stationary Richardson iterations where the relaxation parameter α_k is frozen and set to a value close to $\frac{2}{3}$ for most problems.

Using a Pascal-like notation, the algorithm performs the following steps:

begin
{initialisation step}
$n := 0$;
read in an initial guess $\mathbf{x}^0$;
{Newton's method; variation computation}

repeat

$k := 0$;

{set-up of the initial increment}

$\delta \mathbf{x}_h^0 := (L_{\mathrm{FE}}^n)^{-1}\, \mathbf{b}_h^n$ **or** $\delta \mathbf{x}_h^0 := \mathbf{0}$;

$\delta \mathbf{x}^0 := I_N\, \delta \mathbf{x}_h^0$;

repeat {loop on spectral iteration}

$\mathbf{R} := \mathbf{b}^n - L_C^n\, \delta \mathbf{x}^k$; {residual evaluation}

$\mathbf{R}_h := I_h \mathbf{R}$;

$\delta \mathbf{x}_h^{k+1} := \delta \mathbf{x}_h^k + \alpha_k (L_{\mathrm{FE}}^n)^{-1}\, \mathbf{R}_h$; (5.1)

$\delta \mathbf{x}^{k+1} := I_N\, \delta \mathbf{x}_h^{k+1}$;

$k := k + 1$;

until $\left| \dfrac{\delta \mathbf{x}^k - \delta \mathbf{x}^{k-1}}{\delta \mathbf{x}^k} \right| < \varepsilon_1$ or $\|\mathbf{R}\| < \varepsilon_2$;

{new solution of the nonlinear equations}

$\mathbf{x}^{n+1} := \mathbf{x}^n + \delta \mathbf{x}^k$; (5.2)

$\mathrm{R}_N := L_C^{\mathrm{NS}} \mathbf{x}^{n+1}$;

$n := n + 1$;

until $\left| \dfrac{\mathbf{x}^n - \mathbf{x}^{n-1}}{\mathbf{x}^n} \right|_{\max} < \varepsilon_3$ or $\|\mathbf{R}_N\| < \varepsilon_4$;

end.

In this algorithm, the notation $\delta \mathbf{x}_h^k$ is the finite element solution of the iterative procedure (4.11). As the convergence radius of the Newton's method is small, the solution for a given Reynolds number is obtained through a sequence of runs: first the Stokes solution, followed by intermediate Reynolds number computations. The algebraic solver is a sparse matrix Gaussian elimination with minimum degree ordering [14]. The finite element solver treats the global geometry as a whole (even if subdomain decomposition is used for the Chebyshev approximation). Typically, as the FE solver has a bandwidth of order N, the LU factorisation of L_{FE}^n is performed in $O(N^4)$ operations for this two-dimensional problem. In the other steps of the algorithm, derivatives are computed using fast Chebyshev transforms at a cost of $O(N^2 \log N)$ operations.

6. Domain Decomposition

Inspection of Eq. (4.11) shows that natural boundary conditions are taken easily into account. Therefore for an interior collocation point, the residual will come from the governing equations while for nodal points on $\partial\Omega_n$, both residuals to the equations and natural boundary conditions are used to drive the iterations. This will be the basis for the domain decomposition technique.

The domain Ω is broken up into several subdomains Ω_p, $p = 1, \ldots, L$, which have the following properties:

(i) the sides of every subdomain are parallel to the coordinate axes;

(ii) two subdomains share only one side (or one point);

(iii) the number of degrees of freedom in the direction of the common side must be the same in each adjacent subdomain.

These assumptions lead to conforming finite elements in the preconditioner. Figure 1 displays a typical domain decomposition satisfying these principles.

In each macro-domain Ω_p, a grid $\mathfrak{G}_N^p$ is associated through an affine mapping of the reference square. One has

$$\mathfrak{G}_N = \bigcup_{p=1}^{L} \mathfrak{G}_N^p, \tag{6.1}$$

and, similarly,

$$\mathfrak{G}_{n,N} = \bigcup_{p=1}^{L} \mathfrak{G}_{n,N}^p. \tag{6.2}$$

The space where collocation solutions are sought is defined by

$$\mathscr{P}_N^* = \{v \in C^0(\bar{\Omega}) \mid v|_{\Omega_p} \in \mathscr{P}_{N^p},\ p = 1, ..., L\}, \tag{6.3}$$

where N^p denotes the couple $(N_{x_1}^p, N_{x_2}^p) \in \mathfrak{N} \times \mathfrak{N}$.

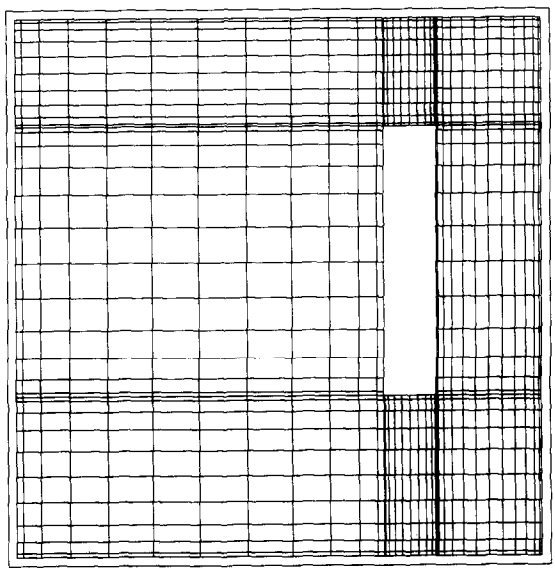

FIG. 1. Square cavity in presence of an obstacle. The subdomain decomposition is adapted to the problem geometry.

The interfaces, i.e., the boundaries of each subdomain Ω_p shared by other subdomains, are denoted by Γ^p and the internal boundary Γ with

$$\Gamma = \bigcup_{p=1}^{L} \Gamma^p. \tag{6.4}$$

The collocation interpolator is extended to the domain decomposition:

$$I_N = \begin{cases} I_N^v : C^0(\bar{\Omega}) \to \mathscr{P}_N^* \\ (I_{2,h}^v \mathbf{v})(\mathbf{r}_i) = \mathbf{v}(\mathbf{r}_i), & \forall \mathbf{r}_i \in \mathfrak{G}_N \\ I_N^q : C^0(\bar{\Omega}) \to \mathscr{P}_N^* \\ (I_N^q q)(\mathbf{r}_i) = q(\mathbf{r}_i), & \forall \mathbf{r}_i \in \mathfrak{G}_N. \end{cases} \tag{6.5}$$

On the internal boundary Γ, one defines the interpolation operator:

$$\mathfrak{I}_h^i = \mathfrak{I}_h(\mathbf{r}_i), \qquad \forall \mathbf{r}_i \in \mathfrak{G}_{2,N} \cap \Gamma. \tag{6.6}$$

The idea of the interface treatment within the domain decomposition [3] is best explained on a scalar model. Let us restrict our attention to the simple problem: Find $u \in H^1(\bar{\Omega})$ such that

$$\begin{aligned} -\Delta u &= f, \qquad \text{on } \Omega, \qquad f \in L^2(\Omega), \\ u(\mathbf{r}) &= 0, \qquad \forall \mathbf{r} \in \partial\Omega, \end{aligned} \tag{6.7}$$

solved by the weak formulation:

$$(\nabla u, \nabla v) = (f, v), \qquad \forall v \in H^1(\Omega). \tag{6.8}$$

By the multidomain decomposition, we wish to solve the problems: Find $u_p \in H^1(\bar{\Omega}_p)$, $p = 1, ..., L$, such that

$$\begin{aligned} -\Delta u_p &= f, && \text{on } \Omega_p, \qquad f \in L^2(\Omega), \\ u_p(\mathbf{r}) &= 0, && \forall \mathbf{r} \in \partial\Omega \\ u_p(\mathbf{r}) &= u_k(\mathbf{r}), && \forall \mathbf{r} \in \Gamma^p \cap \Gamma^k, \\ g_p(\mathbf{r}) &= g_k(\mathbf{r}), && \forall \mathbf{r} \in \Gamma^p \cap \Gamma^k, \end{aligned} \tag{6.9}$$

where g_p represents the flux of u_p across the interface. In this case, the flux is the normal derivative of u_p and is obtained by

$$g_p(\mathbf{r}) = (\nabla u_p \cdot \mathbf{n})(\mathbf{r}), \qquad \forall \mathbf{r} \in \Gamma^p. \tag{6.10}$$

The variational form of (6.9)–(6.10) becomes: Find $u_p \in H^1(\bar{\Omega}_p)$, $p = 1, ..., L$, such that

$$(\nabla u_p, \nabla v_p) = (f, v_p) + \int_{\Gamma^p} g_p(\mathbf{r})\, v_p\, dl, \qquad \forall v_p \in H^1(\Omega_p). \tag{6.11}$$

Summing up the L relationships (6.11), one obtains

$$(\nabla u, \nabla v) = (f, v) + \sum \int_{\Gamma^p} [\, g_p(\mathbf{r})\,]\, v\, dl, \qquad \forall v \in H^1(\Omega), \tag{6.12}$$

where the notation [ ] indicates the jump across the interface of the quantity in between the square brackets. In (6.12), the traces of v_p are supposed to be identical on Γ. Problems (6.8) and (6.12) are equivalent if the sum of interface terms vanish. This is enforced through the relation (6.9).

In the generalization of the previous concepts to the Navier–Stokes equations, the associated flux is the stress vector (2.4). Consequently, the preconditioned scheme of the linearized Navier–Stokes equations may be written as follows:

$$\delta \mathbf{x}^{k+1} = \delta \mathbf{x}^k - \alpha_k I_N (L^n_{\mathrm{FE}})^{-1} [I^c_h (L^n_{\mathrm{C}}\, \delta \mathbf{x}^k - \mathbf{b}^n), \mathfrak{I}_h(\delta \mathbf{t}^k + \mathbf{t}^n - \mathbf{g}_2), \mathfrak{I}^i_h([\delta \mathbf{t}^k + \mathbf{t}^n])]. \tag{6.13}$$

Th C^0 continuity of the flux at convergence (if any) involves the C^1 continuity of the velocities. This can be shown, for example, in Cartesian coordinates considering an interface parallel to the y axis. In this case, the continuity of $\mathbf{t}$ yields the following statements:

$$-p + 2\mu \frac{\partial u}{\partial x} \text{ is continuous,} \tag{6.14}$$

$$\mu \left(\frac{\partial u}{\partial y} + \frac{\partial v}{\partial x} \right) \text{ is continuous.} \tag{6.15}$$

As the pressure is C^0 continuous in the global preconditioner, Eq. (6.14) implies the continuity of $\partial u/\partial x$, while the continuity of $\partial u/\partial y$ ensures that of $\partial v/\partial x$ (6.15). Similar arguments may be developed for an interface parallel to the x axis. One concludes that the velocity field belongs to $H^1(\bar{\Omega})$.

Remark. The present method is not yet applicable to general curvy domains. However, in the spectral approximation, general subdomains can be mapped onto the reference square by transfinite interpolation [15]. The spectral equations are preconditioned by isoparametric elements in order to treat more complicated domains.

7. Numerical Tests for the Mono-domain Algorithm

As a theoretical study of the eigenvalue spectrum of the iteration operator for nonlinear problems is unavailable, the relaxation parameter is set to $\alpha = \frac{2}{3}$ up to a Reynolds number of 1000. For higher Reynolds number values, α is in between 0.55 and 0.4.

An analytical solution of the Navier–Stokes equations is designed in $\Omega = [0, 1] \times [0, 1]$ with $\mu = \rho = 1$. The boundary conditions are imposed via the solution:

$$\begin{aligned} u &= -\cos x \sin y, \\ v &= \sin x \cos y, \\ p &= -2 \sin x \sin y - 0.5(\cos^2 x + \cos^2 y), \\ f_x &= 4 \cos x \sin y, \\ f_y &= 0. \end{aligned} \tag{7.1}$$

The squares of cosine in the pressure will limit the achieved accuracy by the preconditioned collocation method. In each computation, $N_{x_1} = N_{x_2} = N$. Table I gives the maximum error on the velocity components and the pressure, while Table II presents the L_2 norm of the residuals to the momentum and continuity equations. The rate of convergence is indeed exponential.

The next problem is the regularized square cavity already used by Aubert and Deville [1]. The velocity field vanishes on the lateral and bottom walls. The upper side moves in a horizontal plane such that the velocity components are

$$u(x, 1) = 16x^2(x-1)^2, \qquad v(x, 1) = 0, \qquad x \in [0, 1]. \tag{7.2}$$

The Ω domain is the unit square $[0, 1] \times [0, 1]$. The boundary conditions (7.2) smooth out first-order singularities at the top corners which are present in the

TABLE I

Maximum Errors on the Velocities and Pressure as a Function of the Number of Chebyshev Polynomials

N	Maximum error on the velocity components	Maximum error on the pressure
5	1.02 (−5)	4.86 (−4)
7	2.82 (−8)	1.95 (−6)
9	8.59 (−11)	4.71 (−9)
11	1.65 (−13)	9.28 (−12)
13	1.05 (−16)	7.11 (−13)

TABLE II

L-2 Norm of the Residuals to the Momentum and Continuity Equations as a Function of the Number of Chebyshev Polynomials

N	*L*-2 norm of the residuals to the momentum equations	*L*-2 norm of the divergence of the velocity field
5	5.99 (−4)	1.06 (−4)
7	3.40 (−6)	2.88 (−7)
9	1.47 (−8)	8.53 (−10)
11	4.52 (−11)	2.15 (−12)
13	1.24 (−13)	3.82 (−15)

standard square cavity and satisfy the incompressibility condition for $x = 0$ and 1, $y = 1$.

Solutions have been obtained for Reynolds numbers = 0, 100, 1000, 2000, 3500, 4500. Table III reports the minimum value of u along the vertical line across the cavity center and its position. Figure 2 shows the horizontal velocity component along the vertical line located at mid-cavity. Figure 3 exhibits streamlines at Re = 2000, 4500. Table IV presents the numerical values obtained for each vortex. In Fig. 4, for Re = 1000, $N = 29$, the Newton increment $\delta \mathbf{x}^k$ (Eq. (5.2)) is given for the velocity components and the pressure as a function of n, when the initial solution comes from previous Reynolds number calculations (Re = 500). The convergence criterion ε_3 is equal to 10^{-3}. It turns out that after the first iterations, quadratic convergence is achieved by the Newton process. Figure 5 gives for the

TABLE III

For the Regularized Square Cavity Problem, $u_{\min}$ Is the Minimum Value of the Horizontal Velocity Component along the Mid-cavity Vertical Line while $y_{\min}$ Denotes Its Position

N	Re	$u_{\min}$	$y_{\min}$
17	0	−0.1689	0.54855
17	10	−0.16819	0.54727
17	100	−0.163381	0.46613
25	1000	−0.276864	0.20236
25	2000	−0.297964	0.14363
29	3500	−0.311155	0.10911
29	4500	−0.317761	0.09680

Note. $N = N_x = N_y$ yields the number of Chebyshev polynomials used at the Reynolds number Re.

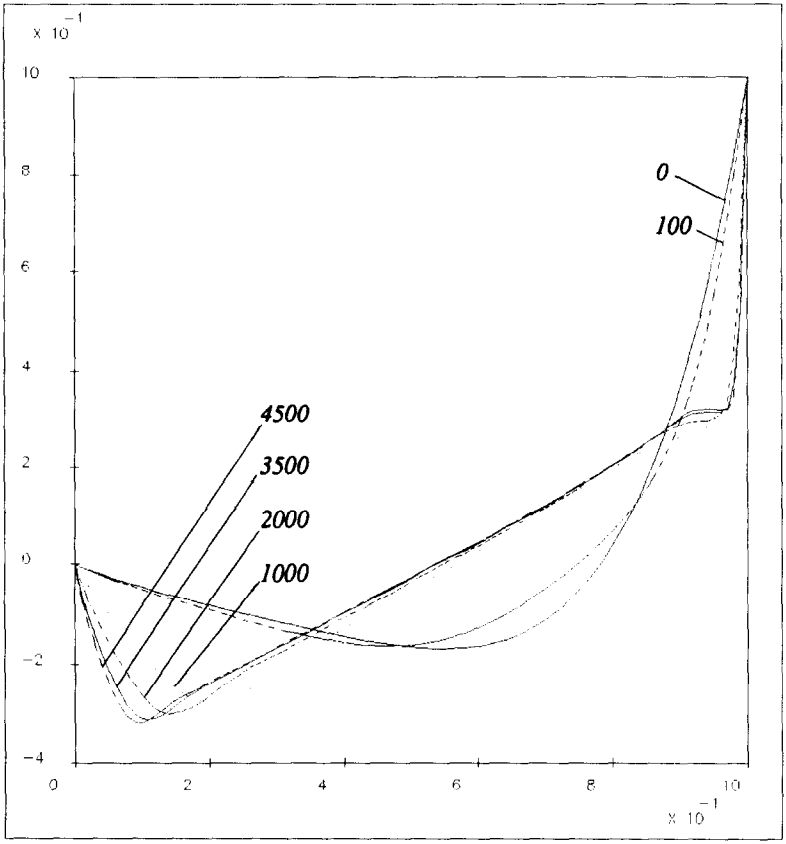

FIG. 2. Horizontal cavity component along the mid-cavity vertical line for Reynolds numbers 0, 100, 1000, 2000, 3500, 4500.

TABLE IV

Properties of Primary and Secondary vortices

		Re	
		2000	4500
Primary	Ψ_{min}	-8.7836×10^{-2}	-8.8756×10^{-2}
	Location x, y	0.5294, 0.5527	0.5206, 0.5391
Top	Ψ_{max}	1.0251×10^{-4}	6.3715×10^{-4}
		0.0411, 0.8911	0.0875, 0.9149
Bottom left	Ψ_{max}	3.5293×10^{-3}	7.8872×10^{-4}
		0.0869, 0.0936	0.0807, 0.1204
Bottom right	Ψ_{max}	1.6062×10^{-3}	2.1204×10^{-3}
		0.8497, 0.1029	0.8141, 0.0825

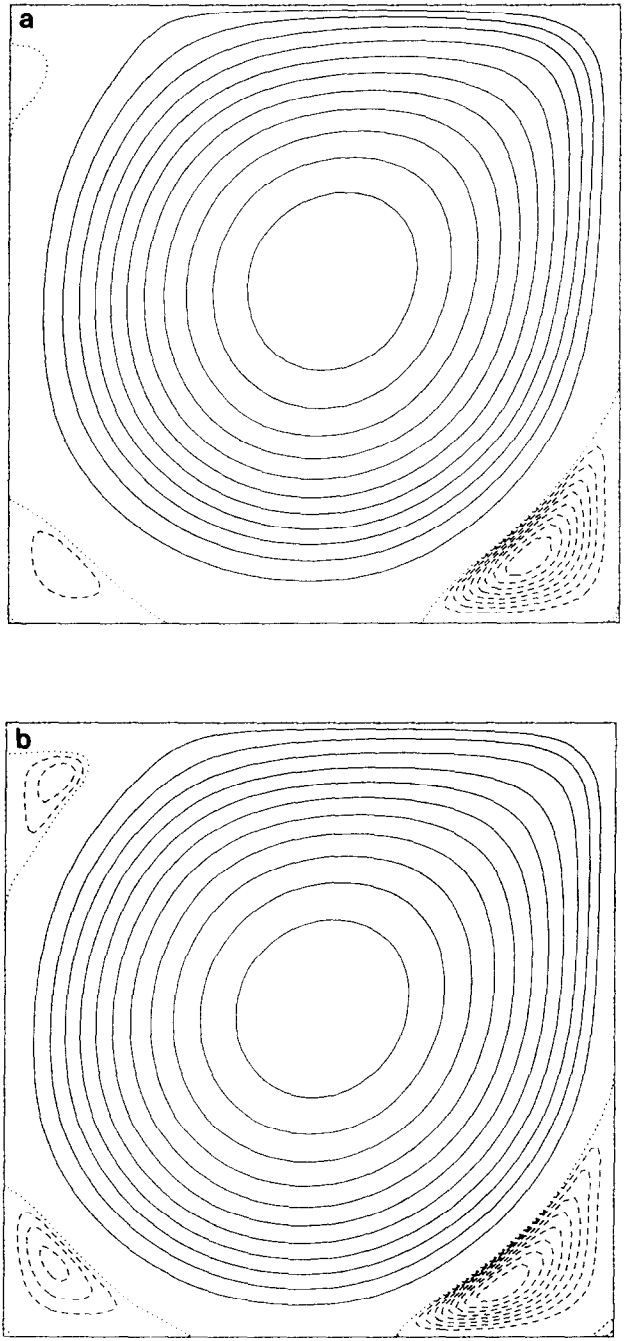

FIG. 3. Streamlines of the regularized square cavity problem at Reynolds number 2000 (a) and 4500 (b).

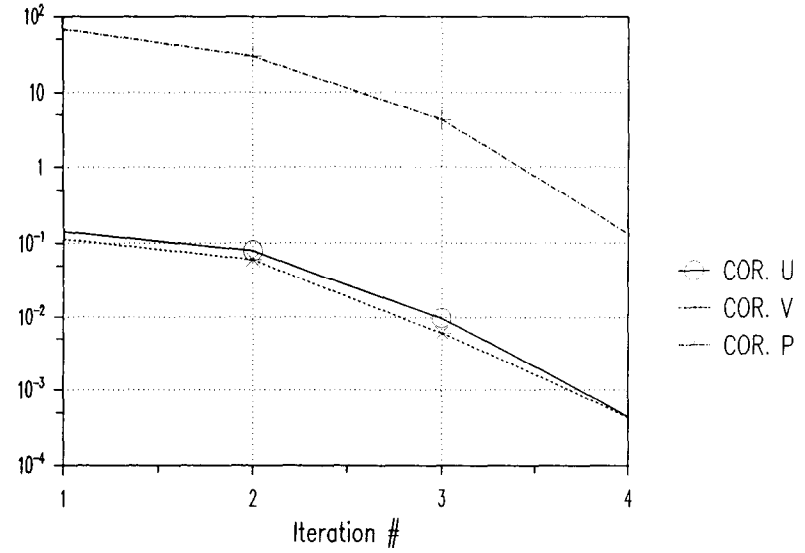

FIG. 4. Evolution of the Newton increment $\delta \mathbf{x}^k$ with respect to the iteration number n for the velocity components and the pressure. The regularized square cavity is solved for Reynolds number 1000 with $N = 29$ and $\alpha_k = 0.5$.

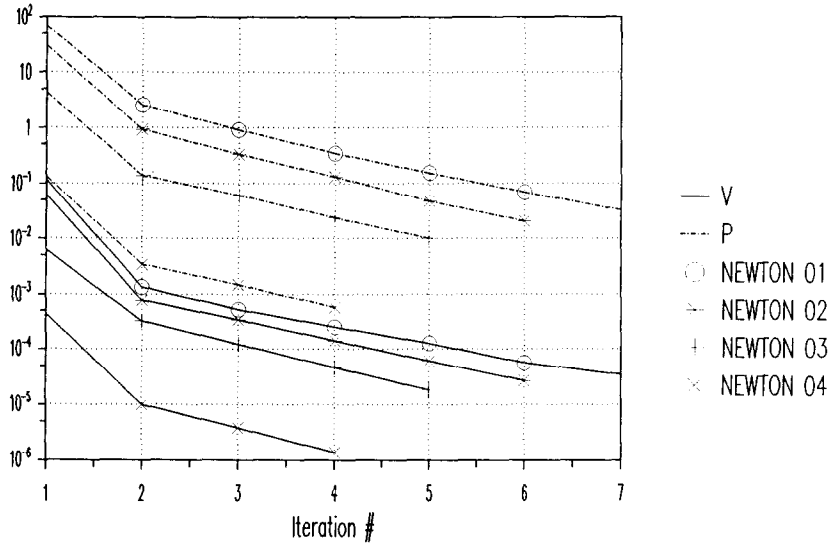

FIG. 5. Evolution of the corrections in the Richardson process for the first four Newton iterations. Same problem as in Fig. 4. The full line is for the vertical velocity component while the dashed line refers to the pressure.

first four Newton iterations the solution of $(L^n_{\mathrm{FE}})^{-1}\,\mathbf{R}_h$ in (5.1) for the pressure and the vertical velocity component. We note that only a few Richardson iterations are needed to advance the solution in this case where $\varepsilon_1 = 10^{-3}$.

8. Numerical Tests for the Multi-domain Algorithm

Let us first consider the convergence of this multi-domain approach on the Stokes equations. The chosen analytical solution is

$$
\begin{aligned}
u &= -\cos\frac{\pi}{2}x \sin\frac{\pi}{2}y,\\
v &= \sin\frac{\pi}{2}x \cos\frac{\pi}{2}y,\\
p &= -\pi \sin\frac{\pi}{2}x \sin\frac{\pi}{2}y,\\
f_x &= \pi^2 \cos\frac{\pi}{2}x \sin\frac{\pi}{2}y,\\
f_y &= 0.
\end{aligned}
\tag{8.1}
$$

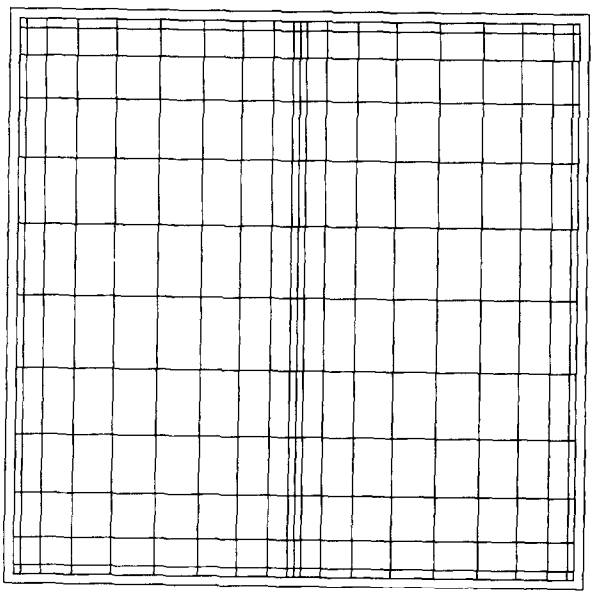

Fig. 6. Decomposition of a unit square with two subdomains of equal size in the x direction.

TABLE V

Maximum Error on the Velocity and Pressure Fields with Respect to the Number of Chebyshev Polynomials

$N_x \times N_y$	Maximum error on the velocities	Maximum error on the pressure
7×13	2.55 (−9)	1.31 (−6)
9×13	1.43 (−12)	7.8 (−10)
11×13	1.36 (−15)	9.49 (−13)
Mono-D		
13×13	5.20 (−15)	1.55 (−11)

Note. The Stokes problem is solved on two equal subdomains in the x direction.

The Ω domain is the unit square and $\mu = 1$. Dirichlet conditions are applied at the walls. The maximum errors on velocities and pressure are recorded for two subdomains of equal size in the x direction (Fig. 6) in Table V and for four equal subdomains (Fig. 7) in Table VI.

For the same number of degrees of freedom, the multidomain computation loses six decades with respect to the mono-domain calculation and requires almost 1.5 times more collocation points in each direction to attain machine accuracy. However, from these tables, we can see that the error decay is still exponential.

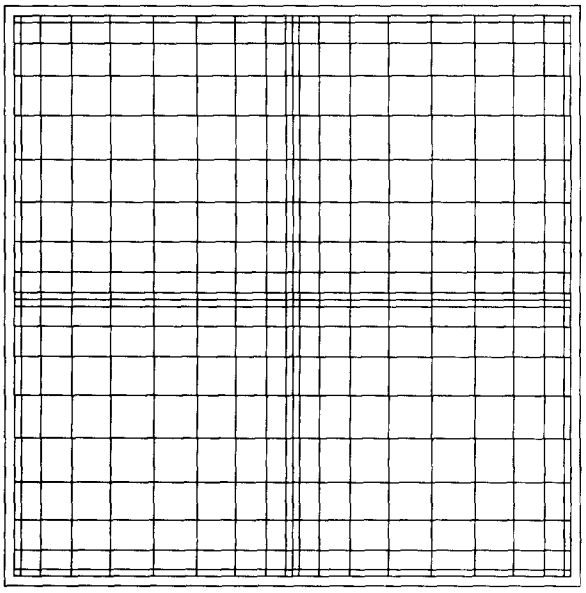

FIG. 7. Decomposition of unit square in four equal subdomains.

TABLE VI

Maximum Error on the Velocity and Pressure Fields with Respect to the Number of Chebyshev Polynomials

$N_x \times N_y$	Maximum error on the velocities	Maximum error on the pressure
7×7	2.97 (−9)	5.33 (−6)
9×9	1.49 (−12)	4.19 (−10)
11×11	7.5 (−16)	9.01 (−13)
Mono-D		
13×13	5.20 (−15)	1.55 (−11)

Note. The Stokes solution is sought on four equal subdomains.

We solve the Navier–Stokes equations for the same analytical solution (8.1) and the same subdivision of the computational domain as before. The results are summarized in Tables VII and VIII and lead to the same conclusions: the multi-domain approach requires more collocation points to reach machine accuracy than the mono-domain algorithm, if the sought solution is smooth enough.

The next problem we want to consider is one where the subdomain decomposition is indispensable because of the geometry. The backward facing step was proposed as a numerical benchmark at a GAMM workshop. A laminar developed profile enters through the inflow section. No-slip boundary conditions are applied on the top and bottom walls and at the outflow section, we shall impose:

$$v = 0, \qquad \frac{\partial u}{\partial x} = 0. \tag{8.2}$$

TABLE VII

Maximum Errors on the Velocity and Pressure Fields versus the Number of Chebyshev Polynomials

$N_x \times N_y$	Maximum error on the velocities	Maximum error on the pressure
7×7	1.76 (−10)	4.52 (−8)
9×9	1.06 (−13)	1.13 (−11)
11×11	2.0 (−15)	7.48 (−12)
Mono-D		
13×13	3.05 (−16)	7.11 (−13)

Note. The Navier–Stokes solution is obtained using two equal subdomains in the x direction.

TABLE VIII

Maximum Errors on the Velocity and Pressure Fields versus the Number of Chebyshev Polynomials

$N_x \times N_y$	Maximum error on the velocities	Maximum error on the pressure
7×7	$1.53(-10)$	$2.33(-8)$
9×9	$1.06(-13)$	$1.28(-11)$
11×11	$5.8(-15)$	$7.26(-12)$
Mono-D 13×13	$3.05(-16)$	$7.11(-13)$

Note. The Navier–Stokes solution is computed using four equal subdomains.

TABLE IX

Comparison of the Maximum Horizontal Component Normalized by u_{max} at Various Cross Sections and of the Length of the Recirculation Zone ($Re = 50$)

X	3.8	5	7	11	Length of the recirculation zone
Min	−0.04	0	0	0	3
Max	0.898	0.772	—	—	
[17]					
Min	−0.046	0	0	0	2.9
Max	0.9098	0.781	0.694	0.668	
Present work					
Min	−0.046	0	0	0	2.9
Max	0.910	0.762	0.694	0.668	
[6]					
Min	−0.035	0	0	0	2.75
Max	0.885	0.78	0.7	0.665	
[16]					
Min	−0.049	0	0	0	3.4
Max	0.914	0.784	0.693	0.669	
[22]					

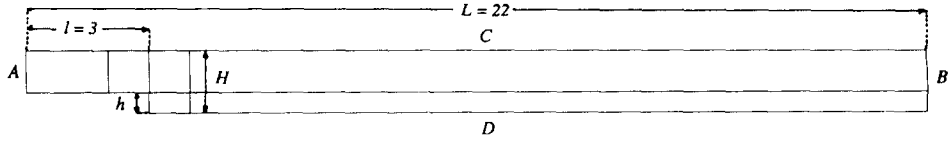

FIG. 8. Geometry of the backward facing step problem.

With $h = 1$ and $H = 1.5$ (Fig. 8), the Reynolds number is defined by the relation:

$$\mathrm{Re} = \frac{u_{\max}(H-h)\,\rho}{\mu}, \tag{8.3}$$

where u_{max} is the maximum value of the entrance velocity profile.

The computational mesh is given on Fig. 9. All subdomains have 11 collocation points in the vertical direction while in the horizontal direction, the number of points goes from 11 to 27. Notice that the corner is chosen on an interface in order to avoid propagating pressure wiggles in the whole domain.

For the Stokes flow, the solution is shown on Fig. 10. Zooming the region around the corner, the geometrical singularity induces isobar lines which are only C^0 continuous at the subdomain interfaces (Fig. 11). At a Reynolds number of 50, Table IX collects the present results and those produced experimentally or by finite element methods. There is excellent agreement between our results and those of Cliffe *et al.* [6]. The fundamental difference is that Cliffe *et al.* used 29,506 degrees of freedom while we used only 3000 d.o.f. Therefore, to reach the same prescribed level of accuracy, the collocation method needs two to three times less degrees of freedom in each space direction than the FE technique. This results in a reduction by a factor 2^4 in the number of operations implied by the LU factorisation and a dramatic saving in computing time for this particular step in the algorithm. We must mention that for problems where there is no corner singularity, e.g., the thermal square cavity [8], the divergence field is at a low level everywhere (10^{-5}—10^{-6}). Across macros boundaries, the divergence is clearly C^0 continuous but not C^1. When geometric singularities are present like in the backward facing step, a loss of 3 to 4 orders of magnitude in the divergence is observed across interfaces of subdomains including that singularity. On Fig. 12, we show the streamlines at $\mathrm{Re} = 50$.

The final test is concerned with a non-simply connected domain. The geometry is shown at Fig. 1. The left corner of the obstacle is at (0.7, 0.3) with respect to the

FIG. 9. Mesh for the backward facing step.

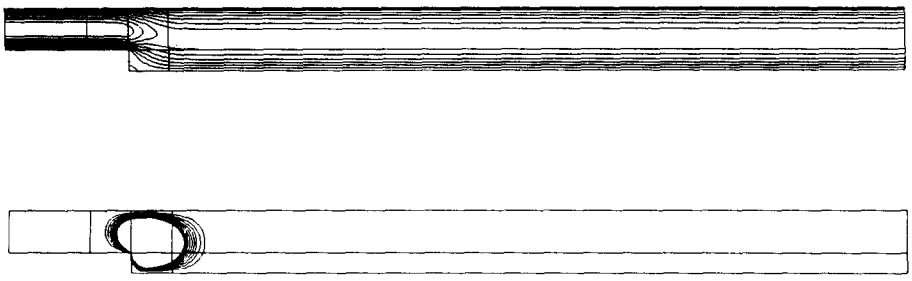

FIG. 10. Isolines of horizontal and vertical velocity components for the Stokes flow.

origin. The width is 0.1 and the height is 0.5. The outer boundary conditions are those of the regularized square cavity. The inner boundary conditions are zero no-slip wall conditions. Numerical results for Reynolds number 100 are shown in Fig. 13. Table X gathers the minimum values of the horizontal velocity component along the mid-cavity vertical line.

9. CONCLUSIONS

A Chebyshev collocation method is proposed to solve the steady Navier–Stokes equations. The collocation method is preconditioned by a finite element technique based on biquadratic velocities and bilinear pressures. A Newton's scheme linearizes the equations and the algorithm is composed essentially of two nested loops: the outer one manages the Newton process and the inner one carries out the Richardson iteration of the preconditioned collocation scheme.

As finite elements easily incorporate natural boundary conditions, a domain decomposition is built up using the jumps of the stress vector at interfaces. Numerical tests on mono-domains demonstrate that the method is able to treat nonlinear problems with a modest discretization. The capabilities of the subdomain decom-

TABLE X

Minimum Value of the Horizontal Velocity Component on the Vertical Line at Mid-cavity in the Presence of an Obstacle

Re	$u_{\min}$
0	−0.12995
10	−0.13237
100	−0.12685

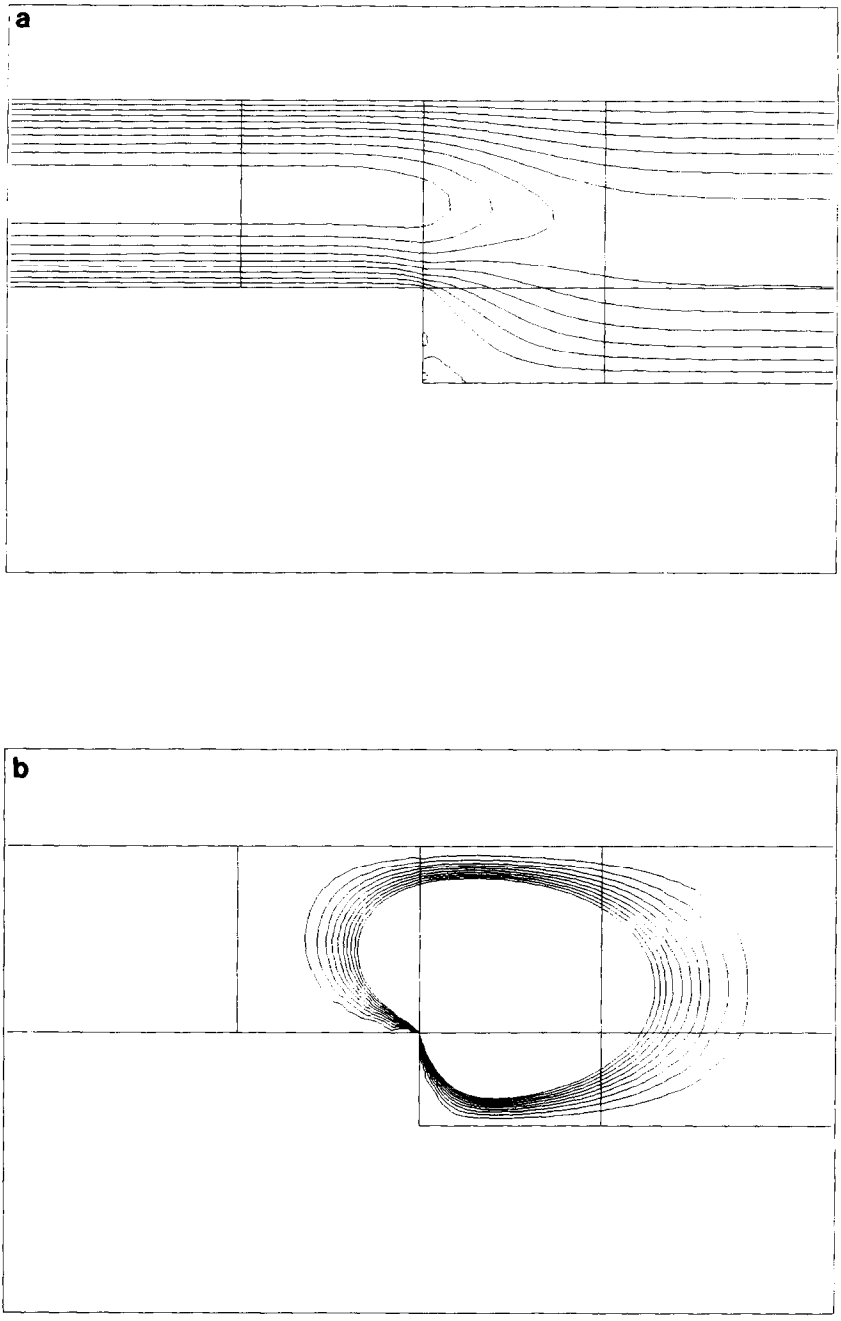

FIG. 11. Blowup of iso-u (a), v (b), and isobars (c) near the corner of the backward facing step for $Re = 0$.

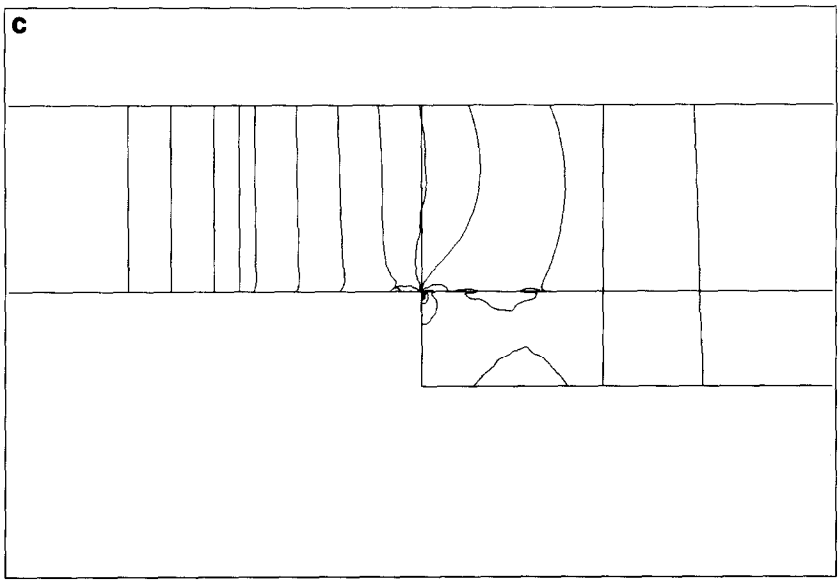

FIG. 11—*Continued*

position are tested on the backward facing step problem and a flow in a cavity presenting an obstacle. The multi-domain algorithm presents the good convergence properties of the mono-domain approach.

The present preconditioning technique may be extended to three-dimensional problems, where triquadratic and trilinear interpolants can be used for the velocities and the pressure, respectively. However, the question of finding the optimal preconditioner remains open because this preconditioner should satisfy the inf–sup condition and provide the solution at a reasonable cost from the computational point of view.

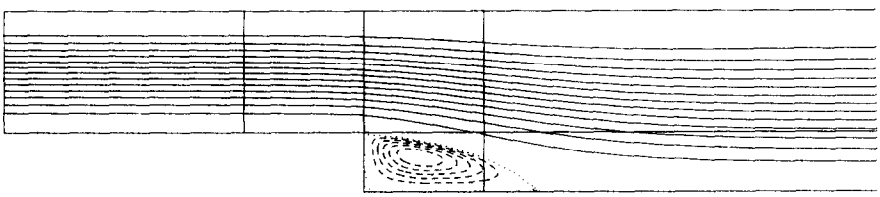

FIG. 12. Streamlines near the corner of the backward facing step, Re = 50.

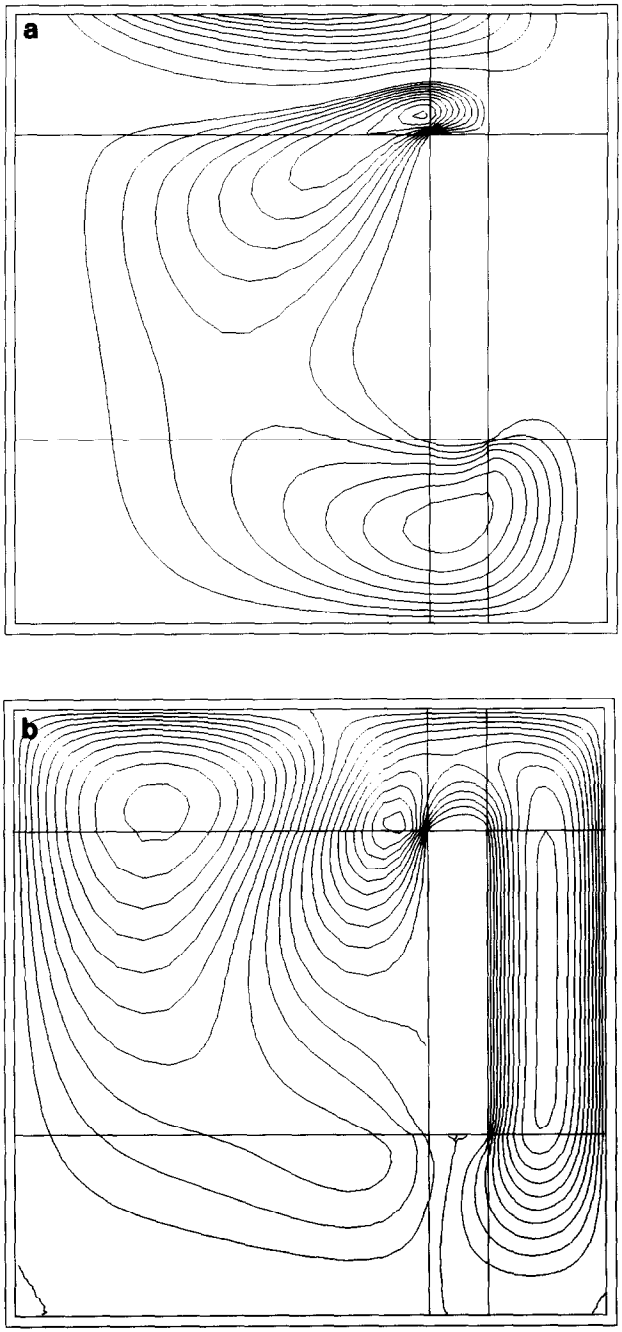

FIG. 13. Isocontours of u (a), v (b), p (c) of the regularized square cavity with an obstacle at $\mathrm{Re} = 100$.

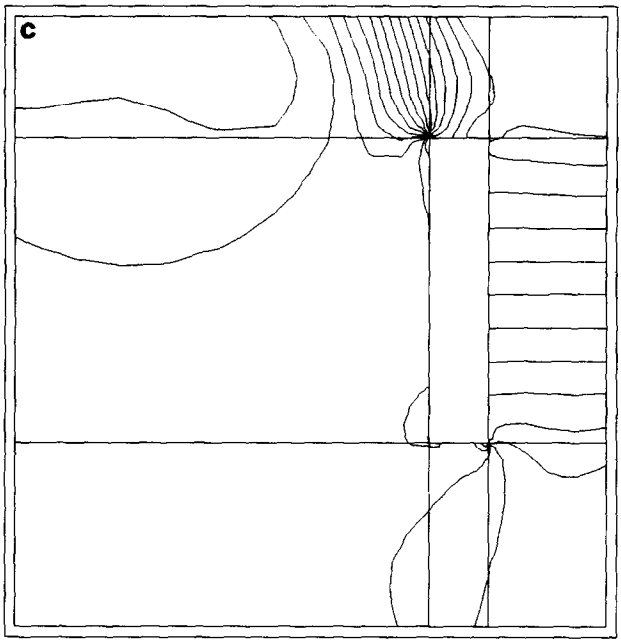

FIG. 13—*Continued*

ACKNOWLEDGMENT

We are indebted to C. Schneidesch who helped us to produce several numerical results and plots for the present study.

REFERENCES

1. X. AUBERT AND M. DEVILLE, *J. Comput. Phys.* **49**, 490 (1983).
2. C. CANUTO, M. Y. HUSSAINI, A. QUARTERONI, AND T. A. ZANG, *Spectral Methods in Fluid Dynamics* (Springer-Verlag, New York, 1988).
3. C. CANUTO AND P. PIETRA, *J. Comput. Phys.* **91**, 310 (1990).
4. C. CANUTO AND A. QUARTERONI, *J. Comput. Phys.* **60**, 315 (1985).
5. P. CIARLET, *The Finite Element Method for Elliptic Problems* (North-Holland, Amsterdam, 1978).
6. K. A. CLIFFE, I. P. JONES, J. D. PORTER, C. P. THOMPSON, AND N. S. WILKES, in *Analysis of Laminar Flow over a Backward Facing Step*, edited by K. Morgan, J. Periaux, and F. Thomasset (Vieweg, Braunschweig, 1984), p. 140.
7. P. DEMARET AND M. O. DEVILLE, *J. Comput. Phys.* **83**, 463 (1989).
8. P. DEMARET, M. O. DEVILLE, AND C. SCHNEIDESCH, *Appl. Numer. Math.* **6**, 107 (1989).
9. P. DEMARET AND M. O. DEVILLE, *Proceedings, 1st Eurotherm Seminar*, edited by H. Meunier (F.P.Ms, Mons, 1988), p. 43.
10. M. O. DEVILLE AND E. H. MUND, *J. Comput. Phys.* **60**, 517 (1985).
11. M. O. DEVILLE AND E. H. MUND, *SIAM J. Sci. Statist. Comput.* **12**, 311 (1990).

12. M. O. DEVILLE AND E. H. MUND, Fourier analysis of finite element preconditioned schemes, *SIAM J. Sci. Statist. Comput.*, to appear.
13. P. HALDENWANG, G. LABROSSE, S. ABOUDI, AND M. DEVILLE, *J. Comput. Phys.* **55**, 115 (1984).
14. A. GEORGE AND J. W. LIU, *SIAM J. Num. Anal.* **17**, 282 (1980).
15. W. J. GORDON AND C. A. HALL, *Numer. Math.* **21**, 109 (1973).
16. J. GOUSSEBAILE, A. HAUGUEL, AND J. M. HERVOUET, in *Analysis of Laminar Flow over a Backward Facing Step*, edited by K. Morgan, J. Periaux, and F. Thomasset (Vieweg, Braunschweig, 1984), p. 268.
17. L. KUENY AND G. BINDER, in *Analysis of Laminar Flow over a Backward Facing Step*, edited by K. Morgan, J. Periaux, and F. Thomasset (Vieweg, Braunschweig, 1984), p. 32.
18. Y. MADAY AND A. T. PATERA, Spectral element methods for the incompressible Navier–Stokes equations, in *State-of-the-Art Surveys on Computational Mechanics*, edited by A. K. Noor and J. T. Oden (ASME, New York, 1989), p. 71.
19. Y. MORCHOISNE, *Rech. Aerosp.* **5**, 293 (1979).
20. S. A. ORSZAG, *J. Comput. Phys.* **37**, 70 (1980).
21. A. J. PATERA, *J. Comput. Phys.* **54**, 468 (1984).
22. J. ROOSE, in *Analysis of Laminar Flow over a Backward Facing Step*, edited by K. Morgan, J. Periaux, F. Thomasset (Vieweg, Braunschweig, 1984), p. 358.